Electrical Engineering (2006) 88: 485–496
DOI 10.1007/s00202-005-0310-6

ORIGINAL PAPER

G. R. Arab Markadeh · J. Soltani

Robust direct torque and flux control of adjustable speed sensorless induction machine drive based on space vector modulation using a PI predictive controller

Received: 15 February 2005 / Accepted: 25 April 2005 / Published online: 24 February 2006

Abstract A Direct torque and flux control design for a sensorless induction motor, following a Lyapunov-based stator flux observer is presented. In this control scheme, the torque error signal and the amplitude of the stator flux reference vector are delivered to a PI predictive controller. The predictive controller also uses information on the amplitude and position of the actual stator flux vector and measured stator currents to determine the voltage command vector for space vector modulation inverter. In addition, a conventional PI speed controller is used to generate the torque reference signal. Using the fifth order model of the three-phase induction machines in a stationary two axes reference frame, a nonlinear stator flux observer is developed in order to estimate the rotor speed, rotor and stator resistances simultaneously. The stability of this observer is proved by Lyapunov theory. It is shown that if the persistancy of excitation condition is satisfied, the estimated quantities converge to their real values. The effectiveness of the proposed control scheme is verified by computer simulation and experimental results.

Keywords Direct torque control · Speed sensorless · Nonlinear stator flux observer · Parameter variation

1 Introduction

The industrial application areas of the direct torque control (DTC) scheme have been increased due to several factors such as quick torque response and robustness against the motor parameter variations [1,2]. The conventional DTC algorithm using the hysteresis based voltage switching method has relative merits of simple structure and easy implementation. The performance of such a scheme depends on the error band set between the desired and measured torque and stator flux values. In addition, in this control scheme, the inverter switching frequency is changed according to the hysteresis bandwidth of flux and torque bang-bang controllers and the variation of speed and motor parameters. Superior motor performance is achieved by narrower hysteresis bands especially in the high speed region. However, these bands cannot be set too small for the protection of the inverter power switching devices. As a result, this approach will not be suitable for high power drives such as those of used in tractions, as they require good torque control performance at considerably lower frequency [3–5]. For such high power industrial applications, if in the DTC, the hysteresis bands of the bang-bang controllers become relatively wide, with the low inverter switching frequency, the resulting motor torque pulsations are high up to an undesired level. In addition to the above drawbacks, the conventional DTC scheme has also other disadvantages such as:

(1) The method causes the switching frequency to vary, giving a continuous harmonic torque ripple especially in the low speed region.
(2) The variation of switching frequency is the drawback of the conventional DTC scheme with digital signal processor (DSP).
(3) The violence of the polarity consistency rules caused by the sector changes, in practice, makes the implementation of the DTC scheme difficult.

To overcome the above problems, so far a few researchers have presented, the DTC scheme using the space vector modulation (SVM) techniques [6,7]. The principles of SM control, DTC and SVM for a sensorless induction motor drive have been combined and applied to a speed sensorless induction motor drive in [6]. Then a conventional two-level space vector PWM inverter is used to indirectly control the IM torque and stator flux magnitude. In addition, the rotor speed is detected by a difference between the estimated angular speed of the rotating rotor flux vector (estimated in the stator two-axis reference frame) and the estimated rotor angular slip speed. The rotor slip speed is given in terms of motor torque and rotor flux magnitude. In [6] the angular speed of

G. R. Arab Markadeh · J. Soltani (✉)
Department of Electrical and Computer Engineering,
Isfahan University of Technology, Isfahan, Iran
Tel.: +98-311-3915383
Fax: +98-311-3912451
E-mail: arab_r@yahoo.com; j1234sm@cc.iut.ac.ir

the stator flux vector is assumed to be equal to the angular speed of the estimated rotor flux vector. This assumption, although correct in steady state condition, is not valid in the induction motor (IM) transient state conditions.

In [7] a control method has been discussed that allows constant switching frequency operation and uses two PI controller in order to generate the inverter reference voltage in the IM stator flux reference frame. In that control scheme, a PI speed controller is also used to obtain the torque reference signal. The control scheme in [7] is not robust to parameters uncertainty, especially to the stator resistance variations. In addition, it is needed to on-line transform the machine variables from a stationary reference frame to the stator flux reference frame and vice-versa.

This paper describes a simple DTC-SVM method for a speed sensorless of induction motor drive. The control method has already been applied to a rotor interior type permanent magnet synchronous motor (IPMSM) [8]. According to this method, a conventional PI predictive controller is used to determine the polar components of the voltage command vector in a stator two-axis reference frame. The error signals between torque and stator flux reference signals and the respected actual values are delivered to the predictive controller. The PI controller also uses the information of the amplitude and position of the estimated stator flux and measured current vectors.

The IM speed sensorless control is another objective of this research work. Elimination of speed sensor increases the reliability of the drive system and decreases the drive costs. The IM speed sensorless schemes are sensitive to motor parameters variation, especially to the rotor and stator resistances that change with temperature and skin effects. In addition, the steady-state error will exist in the rotor or stator flux estimation if these parameters are not perfectly tuned. The error in the IM stator flux estimation is mainly because of stator resistance variation. Noticing that the load dependent variations of the IM windings temperature may lead to up to ±50% error in the stator resistance.

So far many methods such as MRAS-based and observer-based have been proposed for stator resistance estimation [9, 10]. In this paper a novel Lyapunov-based nonlinear stator flux observer is developed for simultaneous estimation of rotor speed, rotor and stator resistances. Using this observer, it will be shown that the estimated quantities converge to their real values if the PE condition is also satisfied. The feasibility of the proposed control approach is supported by simulation and experimental results.

2 IM model

The following equations written in terms of space voltage vector in a stationary reference frame describe the dynamic behavior of an induction motor

$$v_{\mathrm{s}} = R_{\mathrm{s}} i_{\mathrm{s}} + \frac{\mathrm{d}\lambda_{\mathrm{s}}}{\mathrm{dt}} \tag{1}$$

$$0 = R_{\mathrm{r}} i_{\mathrm{r}} + \frac{\mathrm{d}\lambda_{\mathrm{r}}}{\mathrm{dt}} - j\omega_{\mathrm{r}}\lambda_{\mathrm{r}} \tag{2}$$

$$\lambda_{\mathrm{s}} = L_{\mathrm{s}} i_{\mathrm{s}} + L_{\mathrm{m}} i_{\mathrm{r}} \tag{3}$$

$$\lambda_{\mathrm{r}} = L_{\mathrm{r}} i_{\mathrm{r}} + L_{\mathrm{m}} i_{\mathrm{s}} \tag{4}$$

where $v_{\mathrm{s}} = [v_{ds} \;\; v_{qs}]^T$ is space vector of stator voltage, $\lambda_{\mathrm{s}} = [\lambda_{ds} \;\; \lambda_{qs}]^T$ and $\lambda_{\mathrm{r}} = [\lambda_{d\mathrm{r}} \;\; \lambda_{q\mathrm{r}}]^T$ are respectively the stator and rotor flux vectors, $i_{\mathrm{s}} = [i_{ds} \;\; i_{qs}]^T$ and $i_{\mathrm{r}} = [i_{d\mathrm{r}} \;\; i_{q\mathrm{r}}]^T$ are respectively the stator and rotor current vectors. (R_{s}, R_{r}) and (L_{s}, L_{r}) are respectively the stator and rotor resistances and inductances, L_{m} is mutual inductance, ω_{r} is motor angular speed in electrical rad/sec.

Also, the motor mechanical equation is

$$\frac{\mathrm{d}}{\mathrm{dt}}\omega_{\mathrm{m}} = \frac{T_e}{J_{\mathrm{m}}} - \frac{T_l}{J_{\mathrm{m}}} - \frac{B_f}{J_{\mathrm{m}}}\omega_{\mathrm{m}} \tag{5}$$

where $T_{\mathrm{e}\,ref}$ is the motor electromagnetic developed torque which is defined by:

$$T_{\mathrm{e}} = \frac{3}{2}\frac{P}{2}(\lambda_{ds} i_{qs} - \lambda_{qs} i_{ds}) \tag{6}$$

and

P: Number of motor poles
ω_{m}: Rotor mechanical angular speed
ω_{r}: Rotor electrical angular speed
J_{m}: Moment of inertia
B_f: Friction coefficient
T_l: Load torque
T_e: Motor generated torque

By eliminating λ_{r} and i_{r} from Eqs. 1, 2, 3 and 4, the state variable form of the induction motor equations with stator current and rotor flux as state variables becomes

$$\begin{aligned}
\frac{\mathrm{d}}{\mathrm{dt}} i_{ds} &= -\left(\frac{R_{\mathrm{s}}}{\sigma} + \frac{R_{\mathrm{r}}}{L_{\mathrm{r}}} \cdot \frac{L_s}{\sigma}\right) i_{ds} - \omega_{\mathrm{r}} i_{qs} + \frac{R_{\mathrm{r}}}{L_{\mathrm{r}}\sigma}\lambda_{ds} \\
&\quad + \frac{\omega_r}{\sigma}\lambda_{qs} + \frac{1}{\sigma} v_{ds} \\
\frac{\mathrm{d}}{\mathrm{dt}} i_{qs} &= -\left(\frac{R_{\mathrm{s}}}{\sigma} + \frac{R_{\mathrm{r}}}{L_{\mathrm{r}}} \cdot \frac{L_{\mathrm{s}}}{\sigma}\right) i_{qs} + \omega_{\mathrm{r}} i_{ds} + \frac{R_{\mathrm{r}}}{L_{\mathrm{r}}\sigma}\lambda_{qs} \\
&\quad - \frac{\omega_{\mathrm{r}}}{\sigma}\lambda_{ds} + \frac{1}{\sigma} v_{qs} \\
\frac{\mathrm{d}}{\mathrm{dt}}\lambda_{ds} &= -R_s i_{ds} + v_{ds} \\
\frac{\mathrm{d}}{\mathrm{dt}}\lambda_{qs} &= -R_{\mathrm{s}} i_{qs} + v_{qs}
\end{aligned} \tag{7}$$

where $\sigma = L_{\mathrm{s}}(1 - L_{\mathrm{m}}^2 / L_{\mathrm{s}} L_{\mathrm{r}})$ is the motor leakage inductance (or the stator transient inductance).

3 DTC-SVM scheme

Classic DTC methods produce high amounts of current and torque ripples because of switching behavior of torque and

flux controllers and their variable switching frequency. In DTC-SVM method at each cycle period, the calculation of the stator voltage vector is obtained to exactly compensate the stator flux and torque errors. In order to apply this principle, the control system should be able to generate the desired voltage vector, using the space vector modulation technique. One may note that this methodology requires more complex control methods than classic DTC method.

With reference to [11], the fluctuation of the IM torque has a closed relationship to the deviation from an ideal rotation stator flux vector $\lambda_{s\,ref}$, which has a constant rotational speed and a constant length. The difference between $\lambda_{s\,ref}$ and λ_s, which is generated in three-phase PWM inverter, cause torque pulsation. In this case, the tip of the vector goes along a polygon close to a circle as shown in Fig. 1.

The relationship between torque pulsation ΔT_e and the deviation of λ_s from $\lambda_{s\,ref}$ has been deduced as [11]:

$$\frac{\Delta T_e}{T_{e\,ref}} = K_\lambda \frac{|\Delta\lambda_s|}{|\lambda_{s\,ref}|} + K_\delta \Delta\delta \tag{8}$$

where $T_{e\,ref}$ is the steady-state torque and $\Delta\lambda_s$ and $\Delta\delta$ are respectively the deviations from $|\lambda_s|$ and δ which are defined by:

$$\Delta\lambda_s = |\lambda_{s\,ref}| - |\lambda_s| \tag{9}$$

$$\Delta\delta = \angle\lambda_{s\,ref} - \angle\lambda_s \tag{10}$$

and K_δ and K_s are the constants derived from the IM specifications.

The torque ripple is actually caused by $\Delta\lambda_s$ and $\Delta\delta$, and the influences of the $\Delta\lambda_s$ is considerably smaller than that of $\Delta\delta$. As a consequence the torque ripple can be almost removed if $\Delta\delta$ is kept close to zero.

Equation (8) shows that the relation between error of torque and increment angle $\Delta\delta$ is linear. Therefore a PI predictive controller, which generates the load angle changes to minimize the instantaneous error between reference and actual torque, is applied.

Based on Eqs. 8, 9 and 10, the block diagram of Fig. 2a is proposed for DTC-SVM of the three-phase induction motor. From the internal structure of the predictive torque and stator flux controller shown in Fig. 2b, is seen that the torque error, ΔT_e and reference stator flux amplitude, $|\lambda_{s\,ref}|$, are delivered to a mentioned predictive controller which in its output gives the deviation of reference stator flux angle, $\Delta\delta$.

From this figure, the $d:q$ axes components of the stator reference voltage $v_{s\,ref}$, are calculated in the following way:

$$v_{ds\,ref} = \frac{\lambda_{s\,ref}\cos(\delta+\Delta\delta) - \lambda_s\cos(\delta)}{T_s} + R_s i_{ds} \tag{11}$$

$$v_{qs\,ref} = \frac{\lambda_{s\,ref}\sin(\delta+\Delta\delta) - \lambda_s\sin(\delta)}{T_s} + R_s i_{qs} \tag{12}$$

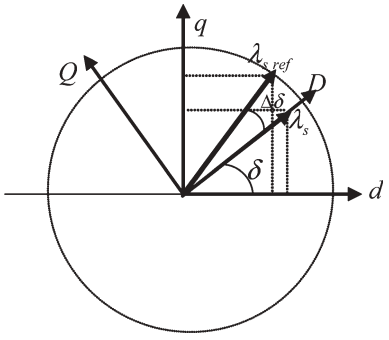

Fig. 1 Stator flux vectors λ_s and $\lambda_{s\,ref}$

4 Nonlinear adaptive stator flux observer

Using the IM model shown in Eq. 7, the following adaptive stator flux observer is proposed.

$$\begin{aligned}
\frac{\mathrm{d}}{\mathrm{dt}}\hat{i}_{ds} &= -\left(\frac{\hat{R}_s}{\sigma} + \frac{\hat{R}_r}{L_r}\cdot\frac{L_s}{\sigma}\right) i_{ds} - \hat{\omega}_r i_{qs} + \frac{\hat{R}_r}{L_r\sigma}\hat{\lambda}_{ds} \\
&\quad + \frac{\hat{\omega}_r}{\sigma}\hat{\lambda}_{qs} + \frac{1}{\sigma}v_{ds} + f_d \\
\frac{\mathrm{d}}{\mathrm{dt}}\hat{i}_{qs} &= -\left(\frac{\hat{R}_s}{\sigma} + \frac{\hat{R}_r}{L_r}\cdot\frac{L_s}{\sigma}\right) i_{qs} + \hat{\omega}_r i_{ds} + \frac{\hat{R}_r}{L_r\sigma}\hat{\lambda}_{qs} \\
&\quad - \frac{\hat{\omega}_r}{\sigma}\hat{\lambda}_{ds} + \frac{1}{\sigma}v_{qs} + f_q \\
\frac{\mathrm{d}}{\mathrm{dt}}\hat{\lambda}_{ds} &= -\hat{R}_s i_{ds} + v_{ds} + \sigma f_d \\
\frac{\mathrm{d}}{\mathrm{dt}}\hat{\lambda}_{qs} &= -\hat{R}_s i_{qs} + v_{qs} + \sigma f_q
\end{aligned} \tag{13}$$

where ^ means the estimated value of each state and parameter and f_d and f_q will be defined later.

In order to develop the adaptation laws, it is assumes that the motor speed, rotor and stator resistances are unknown constant parameters. Having assumed that, from Eqs. 7 and 13 the observer error dynamic is expressed by

$$\begin{aligned}
\frac{\mathrm{d}}{\mathrm{dt}}\tilde{i}_{ds} &= -\left(\frac{\tilde{R}_s}{\sigma} + \frac{\tilde{R}_r}{L_r}\cdot\frac{L_s}{\sigma}\right) i_{ds} - \tilde{\omega}_r i_{qs} + \frac{R_r}{L_r\sigma}\tilde{\lambda}_{ds} \\
&\quad + \frac{\tilde{R}_r}{L_r\sigma}\hat{\lambda}_{ds} + \frac{\omega_r}{\sigma}\tilde{\lambda}_{qs} + \frac{\tilde{\omega}_r}{\sigma}\hat{\lambda}_{qs} - f_d \\
\frac{\mathrm{d}}{\mathrm{dt}}\tilde{i}_{qs} &= -\left(\frac{\tilde{R}_s}{\sigma} + \frac{\tilde{R}_r}{L_r}\cdot\frac{L_s}{\sigma}\right) i_{qs} + \tilde{\omega}_r i_{ds} + \frac{R_r}{L_r\sigma}\hat{\lambda}_{qs} \\
&\quad + \frac{\tilde{R}_r}{L_r\sigma}\hat{\lambda}_{qs} - \frac{\omega_r}{\sigma}\tilde{\lambda}_{ds} - \frac{\tilde{\omega}_r}{\sigma}\hat{\lambda}_{ds} - f_q \\
\frac{\mathrm{d}}{\mathrm{dt}}\tilde{\lambda}_{ds} &= -\tilde{R}_s i_{ds} - \sigma f_d \\
\frac{\mathrm{d}}{\mathrm{dt}}\tilde{\lambda}_{qs} &= -\tilde{R}_s i_{qs} - \sigma f_q
\end{aligned} \tag{14}$$

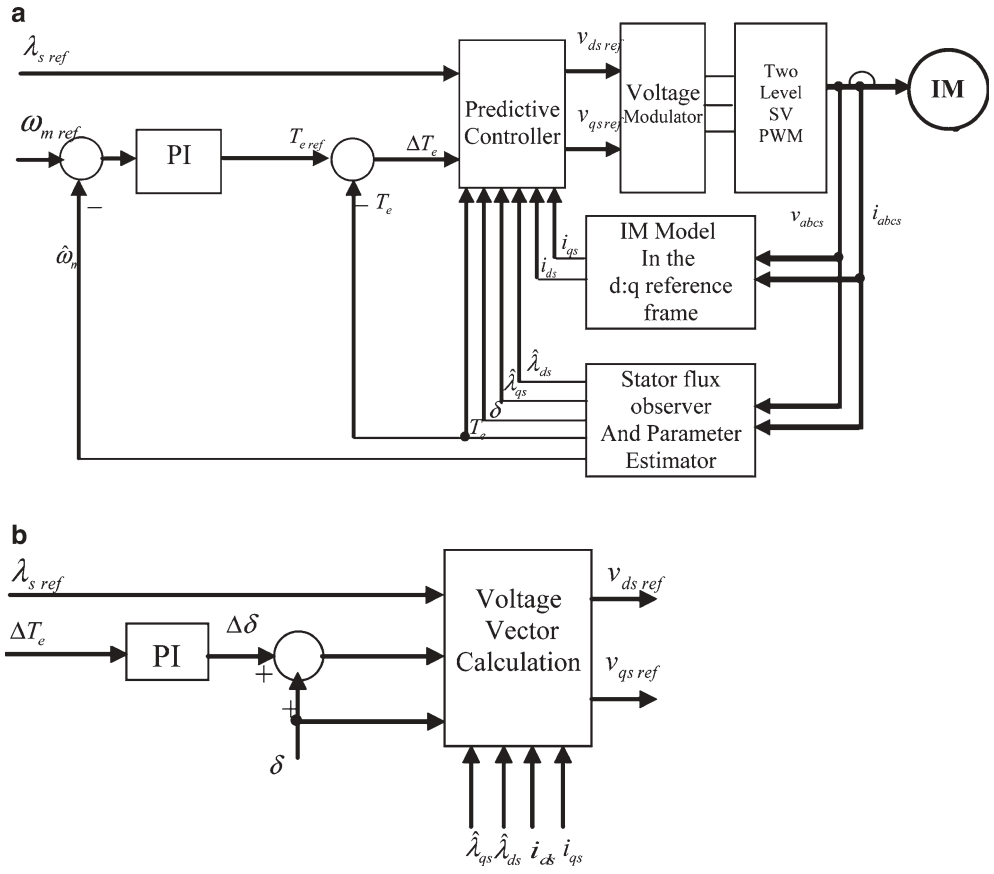

Fig. 2 **a** Induction motor (IM) drive system control. **b** PI predictive controller

where,

$$\tilde{i}_{ds} = i_{ds} - \hat{i}_{ds}, \quad \tilde{i}_{qs} = i_{qs} - \hat{i}_{qs}, \quad \tilde{\lambda}_{ds} = \lambda_{ds} - \hat{\lambda}_{ds},$$
$$\tilde{\lambda}_{qs} = \lambda_{qs} - \hat{\lambda}_{qs}, \quad \tilde{R}_s = R_s - \hat{R}_s, \quad \tilde{R}_r = R_r - \hat{R}_r,$$
$$\tilde{\omega}_r = \omega_r - \hat{\omega}_r$$

The adaptation laws for uncertain parameters and the auxiliary known functions of f_d and f_q, should be designed so that the current estimation errors asymptotically converge to zero. In order to obtain a state variable which is independent of uncertain parameters, the following variables are defined

$$z_d = \tilde{\lambda}_{ds} + \int_0^t \tilde{R}_s i_{ds} \mathrm{d}t$$
$$z_q = \tilde{\lambda}_{qs} + \int_0^t \tilde{R}_s i_{qs} \mathrm{d}t \tag{15}$$

Linking Eqs. 14 and 15, gives

$$\frac{\mathrm{d}}{\mathrm{d}t} z_d = -\sigma f_d$$
$$\frac{\mathrm{d}}{\mathrm{d}t} z_q = -\sigma f_q \tag{16}$$

Because of unknown initial values of $\tilde{z}_d(0) = z_d(0) - \hat{z}_d(0)$ and $\tilde{z}_q(0) = z_q(0) - \hat{z}_q(0)$ there is no guarantee for $\tilde{z}_d$ and $\tilde{z}_q$ to be asymptotic stable; to solve this problem, the following additional state variables are introduced

$$\eta_d = \tilde{z}_d = z_d - \hat{z}_d$$
$$\eta_q = \tilde{z}_q = z_q - \hat{z}_q \tag{17}$$

Substituting Eqs. 15, 16, and 17 in Eq. 14, the observer dynamic is obtained as

$$\begin{aligned}
\frac{\mathrm{d}}{\mathrm{d}t}\tilde{i}_{ds} &= -k_d \tilde{i}_{ds} - \omega_r \tilde{i}_{qs} \\
&+ \frac{1}{\sigma}\left[-L_s i_{ds} + \hat{z}_d + \int_0^t \hat{R}_s i_{ds}\,\mathrm{d}t + \hat{\lambda}_{ds}\right]\frac{\tilde{R}_r}{L_r} - \frac{i_{ds}}{\sigma}\tilde{R}_s \\
&- \frac{q_{ds}}{\sigma L_r}\tilde{R} - \frac{q_{qs}}{\sigma}\tilde{R}_\omega + \frac{R_r}{\sigma L_r}\tilde{z}_d + \frac{\omega_r}{\sigma}\tilde{\eta}_q \\
&+ \frac{1}{\sigma}\left[-\sigma i_{qs} + \hat{z}_q + \hat{\eta}_q + \int_0^t \hat{R}_s i_{qs}\,\mathrm{d}t + \hat{\lambda}_{qs}\right]\tilde{\omega}_r \\
\frac{\mathrm{d}}{\mathrm{d}t}\tilde{i}_{qs} &= -k_q \tilde{i}_{qs} + \omega_r \tilde{i}_{ds} \\
&+ \frac{1}{\sigma}\left[-L_s i_{qs} + \hat{z}_q + \int_0^t \hat{R}_s i_{qs}\,\mathrm{d}t + \hat{\lambda}_{qs}\right]\frac{\tilde{R}_r}{L_r} - \frac{i_{qs}}{\sigma}\tilde{R}_s \\
&- \frac{q_{qs}}{\sigma L_r}\tilde{R} + \frac{q_{ds}}{\sigma}\tilde{R}_\omega + \frac{R_r}{\sigma L_r}\tilde{z}_q - \frac{\omega_r}{\sigma}\tilde{\eta}_d \\
&- \frac{1}{\sigma}\left[-\sigma i_{ds} + \hat{z}_d + \hat{\eta}_d + \int_0^t \hat{R}_s i_{ds}\,\mathrm{d}t + \hat{\lambda}_{ds}\right]\tilde{\omega}_r
\end{aligned} \tag{18}$$

with

$$
\begin{aligned}
f_d &= k_d\tilde{i}_{ds} - \omega_r\tilde{i}_{qs} + \left[\hat{z}_d + \int_0^t \hat{R}_s i_{ds}\,\mathrm{d}t\right]\frac{\hat{R}_r}{\sigma L_r} - \frac{q_{ds}}{\sigma L_r}\hat{R} \\
&\quad -\frac{q_{qs}}{\sigma}\hat{R}_\omega + \frac{1}{\sigma}\left[\hat{z}_q + \hat{\eta}_q + \int_0^t \hat{R}_s i_{qs}\,\mathrm{d}t\right]\hat{\omega}_r \\
f_q &= k_q\tilde{i}_{qs} + \omega_r\tilde{i}_{ds} + \left[\hat{z}_q + \int_0^t \hat{R}_s i_{qs}\,\mathrm{d}t\right]\frac{\hat{R}_r}{\sigma L_r} \\
&\quad -\frac{q_{qs}}{\sigma L_r}\hat{R} + \frac{q_{ds}}{\sigma}\hat{R}_\omega - \frac{1}{\sigma}\left[\hat{z}_d + \hat{\eta}_d + \int_0^t \hat{R}_s i_{ds}\,\mathrm{d}t\right]\hat{\omega}_r
\end{aligned}
\tag{19}
$$

where q_{ds} and q_{qs} are assumed bounded variables defined by:

$$
\begin{aligned}
q_{ds} &= \int_0^t i_{ds}\,\mathrm{d}t \\
q_{qs} &= \int_0^t i_{qs}\,\mathrm{d}t
\end{aligned}
\tag{20}
$$

and $R = R_s \cdot R_r$, $R_w = R_s \cdot \omega_r$, $\tilde{R} = R - \hat{R}$, $\tilde{R}_\omega = R_\omega - \hat{R}_\omega$ and k_d and k_q are positive observer gains.

Equation 18 in matrix form, becomes

$$
\dot{x} = Ax + W^T\tilde{\theta} \tag{21}
$$

where

$$
x = \left[\tilde{i}_{ds}, \tilde{i}_{qs}\right]^T, \quad \tilde{\theta} = \left[\tilde{R}_r, \tilde{R}_s, \tilde{R}, \tilde{R}_w, \tilde{\omega}_r, \tilde{z}_d, \tilde{z}_q, \tilde{\eta}_d, \tilde{\eta}_q\right]^T
$$

$$
A = \begin{bmatrix} -k_d & -\omega_r \\ \omega_r & -k_q \end{bmatrix}
$$

and

$$
W^T = \begin{bmatrix}
\frac{1}{\sigma L_r}\left[-L_s i_{ds} + \hat{z}_d + \int_0^t \hat{R}_s i_{ds}\,\mathrm{d}t + \hat{\lambda}_{ds}\right] & -\frac{i_{ds}}{\sigma} & -\frac{q_{ds}}{\sigma L_r} & -\frac{q_{qs}}{\sigma} & \frac{1}{\sigma}\left[-\sigma i_{qs} + \hat{z}_q + \hat{\eta}_q + \int_0^t \hat{R}_s i_{qs}\,\mathrm{d}t + \hat{\lambda}_{qs}\right] & \frac{R_r}{\sigma L} & 0 & 0 & \frac{\omega_r}{\sigma} \\
\frac{1}{\sigma L_r}\left[-L_s i_{qs} + \hat{z}_q + \int_0^t \hat{R}_s i_{qs}\,\mathrm{d}t + \hat{\lambda}_{qs}\right] & -\frac{i_{qs}}{\sigma} & -q_{qs} & \sigma L_r\frac{q_{ds}}{\sigma} & -\frac{1}{\sigma}\left[-\sigma i_{ds} + z_d + \hat{\eta}_d + \int_0^t \hat{R}_s i_{ds}\,\mathrm{d}t + \hat{\lambda}_{ds}\right] & 0 & \frac{R_r}{\sigma L} & \frac{-\omega_r}{\sigma} & 0
\end{bmatrix}
\tag{22}
$$

Candidate the following Lyapunov function

$$
V = \frac{1}{2}x^T x + \frac{1}{2}\tilde{\theta}^T\Gamma^{-1}\tilde{\theta} \tag{23}
$$

where

$$
\Gamma{=}\mathrm{diag}\left[\sigma L_r\gamma_r, \sigma\gamma_s, \sigma L_r\gamma_R, \sigma\gamma_{R\omega}, \sigma\gamma_\omega, \sigma L_r\gamma_z, \sigma L_r\gamma_z, \frac{\sigma}{\omega_r}\gamma_\eta, \frac{\sigma}{\omega_r}\gamma_\eta\right]
$$

The adaptation gains, γ_R, γ_s, γ_r, $\gamma_{R\omega}$, γ_ω, γ_z, γ_η are positive constants.

Note that W and Γ include the unknown parameters R_r and ω_r, which are canceled when W is multiplied by Γ.

Derivating function V with respect to time, yields

$$
\dot{V} = x^T Ax + \tilde{\theta}^T Wx + \tilde{\theta}^T\Gamma^{-1}\dot{\tilde{\theta}} \tag{24}
$$

Assume the adaptation law as

$$
\dot{\tilde{\theta}} = -\Gamma Wx \tag{25}
$$

Then

$$
\dot{V} = x^T Ax \tag{26}
$$

Since A is also a negative definite matrix, then from (26), yields

$$
\dot{V} < 0 \tag{27}
$$

In addition since R_r, R_s, R, R_ω, ω_r are assumed unknown constant parameters, then

$$
\begin{aligned}
&\dot{\tilde{R}}_r = -\dot{\hat{R}}_r, \quad \dot{\tilde{R}}_s = -\dot{\hat{R}}_s, \quad \dot{\tilde{R}} = -\dot{\hat{R}}, \\
&\dot{\tilde{R}}_\omega = -\dot{\hat{R}}_\omega, \quad \dot{\tilde{\omega}}_r = -\dot{\hat{\omega}}_r, \quad \dot{\tilde{z}}_d = -\sigma f_d - \dot{\hat{z}}_d, \\
&\dot{\tilde{z}}_q = -\sigma f_q - \dot{\hat{z}}_q, \quad \dot{\tilde{\eta}}_d = \dot{\tilde{z}}_d - \dot{\hat{\eta}}_d \text{ and } \dot{\tilde{\eta}}_q = \dot{\tilde{z}}_q - \dot{\hat{\eta}}_q
\end{aligned}
\tag{28}
$$

As a result, from Eqs. 25 and 28, the adaptation laws are obtained as

$$
\begin{aligned}
\dot{\hat{R}}_r &= \gamma_r\left[\left(-L_s i_{ds} + \hat{z}_d + \int_0^t \hat{R}_s i_{ds}\,\mathrm{d}t + \hat{\lambda}_{ds}\right)\tilde{i}_{ds}\right. \\
&\quad \left. + \left(-L_s i_{qs} + \hat{z}_q + \int_0^t \hat{R}_s i_{qs}\,\mathrm{d}t + \hat{\lambda}_{qs}\right)\tilde{i}_{qs}\right] \\
\dot{\hat{R}}_s &= -\gamma_s\left[i_{ds}\tilde{i}_{ds} + i_{qs}\tilde{i}_{qs}\right] \\
\dot{\hat{R}} &= -\gamma_R\left[q_{ds}\tilde{i}_{ds} + q_{qs}\tilde{i}_{qs}\right] \\
\dot{\hat{R}}_\omega &= -\gamma_{R\omega}\left[q_{qs}\tilde{i}_{ds} - q_{ds}\tilde{i}_{qs}\right] \\
\dot{\hat{\omega}}_r &= \gamma_\omega\left[\left(-\sigma i_{qs} + \hat{z}_q + \hat{\eta}_q + \int_0^t \hat{R}_s i_{qs}\,\mathrm{d}t + \hat{\lambda}_{qs}\right)\tilde{i}_{ds}\right. \\
&\quad \left. - \left(-\sigma i_{ds} + \hat{z}_d + \hat{\eta}_d + \int_0^t \hat{R}_s i_{ds}\,\mathrm{d}t + \hat{\lambda}_{ds}\right)\tilde{i}_{qs}\right]
\end{aligned}
\tag{29}
$$

$$
\begin{aligned}
\dot{\hat{z}}_d &= -\sigma f_d + \gamma_z\tilde{i}_{ds} \\
\dot{\hat{z}}_q &= -\sigma f_q + \gamma_z\tilde{i}_{qs} \\
\dot{\hat{\eta}}_d &= -\gamma_z\tilde{i}_{ds} - \gamma_\eta\tilde{i}_{qs} \\
\dot{\hat{\eta}}_q &= -\gamma_z\tilde{i}_{qs} + \gamma_\eta\tilde{i}_{ds}
\end{aligned}
$$

Since V is a radially unbounded function, Eqs. 27 and 28 guarantee that $\tilde{i}_{ds}, \tilde{i}_{qs}, \tilde{R}_r, \tilde{R}_s, \tilde{R}, \tilde{R}_w, \tilde{\omega}_r, \tilde{z}_d, \tilde{z}_q, \tilde{\eta}_d$ and $\tilde{\eta}_q$ are bounded. In addition, since $\int_0^t i_{ds}\,\mathrm{d}t$ and $\int_0^t i_{qs}\,\mathrm{d}t$ are assumed to be bounded, $\int_0^t \tilde{R}_s i_{ds}\,\mathrm{d}t$, $\int_0^t \tilde{R}_s i_{qs}\,\mathrm{d}t$, $\int_0^t \hat{R}_s i_{ds}\,\mathrm{d}t$ and $\int_0^t \hat{R}_s i_{qs}\,\mathrm{d}t$ are also bounded. As a consequence of Eq. 29, $\hat{\lambda}_{ds}, \hat{\lambda}_{ds}, \hat{z}_d, \hat{z}_q, \hat{\eta}_d, \hat{\eta}_q$ must also be bounded. That means from Eq. 21, W^T and $\dot{x}$ also have to bounded. As a result, from Barbalat's lemma, it follows that

$$
\lim_{t\to\infty}\tilde{i}_{ds} = 0, \lim_{t\to\infty}\tilde{i}_{qs} = 0 \tag{30}
$$

Moreover, the PE condition implies that there exists some $T > 0$ such that for any $t > 0$, $\int_t^{t+T} W(\tau)W^T(\tau)\mathrm{d}\tau \geq cI > 0$,

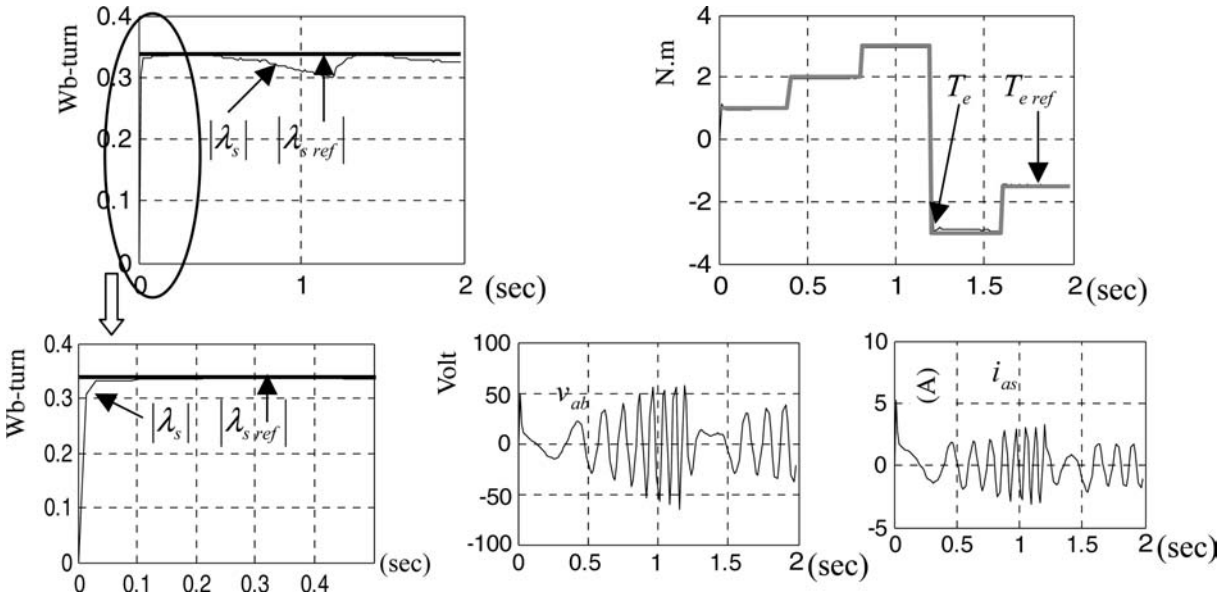

Fig. 3 Simulation results: IM torque control

the estimation error vector $\tilde{\theta}$ will converge exponentially to zero [12].

In [13], it is explained that for simultaneous estimation of the IM speed and rotor resistance, if a low frequency, low amplitude ac signal (or combination of them), is superimposed on to the rotor reference flux, then PE condition is satisfied even in steady-state condition. It must be noted that in a light load torque, where the rotor current is small, simultaneous estimation of the stator and rotor resistances cannot be achieved [14]. That is because the PE condition is not then satisfied.

It is not difficult to show that if the estimation error vector, $\tilde{\theta}$, exponentially tends to zero, then $\tilde{\lambda}_{ds}$ and $\tilde{\lambda}_{qs}$ also exponentially converges to zero. That means $\lim_{t\to\infty} \tilde{\lambda}_{ds} = 0$, $\lim_{t\to\infty} \tilde{\lambda}_{qs} = 0$.

5 System simulation

The proposed nonlinear control torque and stator flux were first investigated by simulations. The overall control block diagram is shown in Fig. 2. According to this figure, the IM drive is supplied by a two level SV-PWM inverter.

Table 1 Induction motor parameters

Power	2.5 kW
R_r	1.8 Ω
R_s	3.55 Ω
Pole	4
L_m	301.6 mH
L_r	311.6 mH
L_s	311.6 mH
J_m	0.02 kg m^2

A C^{++} computer program was developed to model the system control shown in Fig. 2. In this program a static Runge-Kutta fourth order method is used to solve the system equations. Using this program, the stator current and stator flux components are obtained by solving the nonlinear equations (Eq. 7). The characteristics of the simulated motor are shown in Table 1.

Based on the implemented system and considering the computing time, the reasonable sampling period for the proposed nonlinear adaptive controller is chosen to be 200 μs. Additionally, in order to satisfy the system PE condition, an ac small signal with amplitude of 0.02 Wb-turns and frequency of about 3.5 Hz is superimposed on to the stator reference flux. Also in order to achieve a reasonably high performance system, the observer adaptation gains are chosen as $\gamma_r = 0.7$, $\gamma_s = 0.4$, $\gamma_R = 10$, $\gamma_{R\omega} = 10$, $\gamma_\omega = 50$, $\gamma_z = 0.001$, $\gamma_\eta = 0.01$, and $k_d = k_q = 350$. Moreover the coefficients of the conventional motor speed and predictive PI controllers respectively are chosen as (Kp=0.03, K_I=0.01) and (Kp=0.003, K_I=1). Noting that the values of the above coefficients are obtained based on trial and error through some sensitivity simulation tests which are carried out with respect to coefficient variation. The sensitivity tests show that the system performance is more affected by the variations in γ_r and γ_ω than in the other coefficients. That is because an error in rotor resistance estimation will cause a considerable error in rotor speed estimation and vice-versa. In addition, our sensitivity tests also show that γ_s and γ_ω coefficients have considerable effects on the IM drive performance especially in the IM low speed operating region.

Figure 3 shows the simulated results obtained for the IM torque control in the case of a step up stator reference flux from 0 to λ_s =0.33 Wb-turns at t=0 s and a step up and step down torque reference profile which is also depicted in Fig. 3.

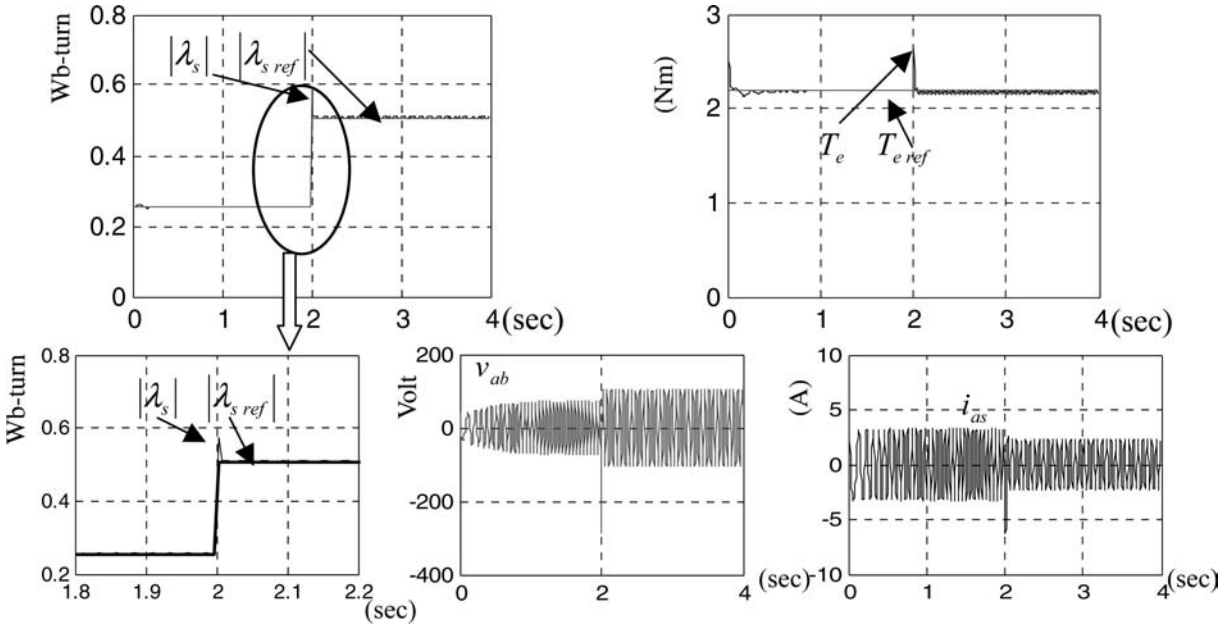

Fig. 4 Simulation results: IM stator flux control

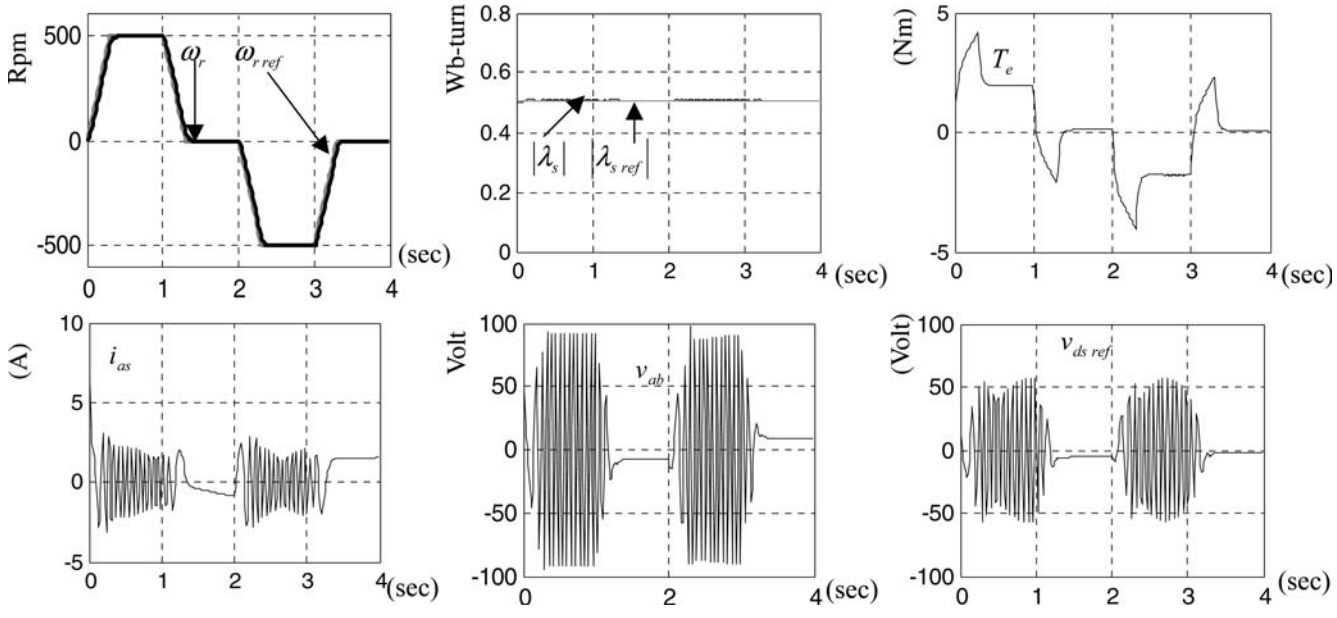

Fig. 5 Simulation results: IM speed control

The IM stator flux control is shown in Fig. 4. The results of Fig. 4 are obtained in the case of a step up and step down stator reference flux linkages respectively from 0 to 0.25 Wb-turns at t=0 s and from 0.25 to 0.5 Wb-turns at t=2 s.

The IM four quadrant speed control response obtained for a step up stator reference flux from 0 to 0.5 Wb-turn at t=0 s is shown in Fig. 5.

Using the nonlinear adaptive stator flux observer described in Sect. 4, assuming the initial errors of +30 and −40% respectively in the stator and rotor resistances, the simulated results shown in Fig. 6 are obtained in the case of a step up stator flux reference from 0 to 0.6 Wb-turns at t=0 sec, and an exponential speed reference command from 0 to 500 rpm at t=0 s. In addition, the stator flux observer behavior due to the initial errors of −30 and −40% respectively in the stator and rotor resistances and an exponential speed reference command from 0 to 50 rpm at t=0 s are demonstrated in Fig. 7. From these results one can see that the estimated errors in the speed and motor resistances asymptotically converge to zero. In Fig. 6 it is seen that the estimated stator resistance decreases towards its actual value. That is because this parameter is initially overestimated to

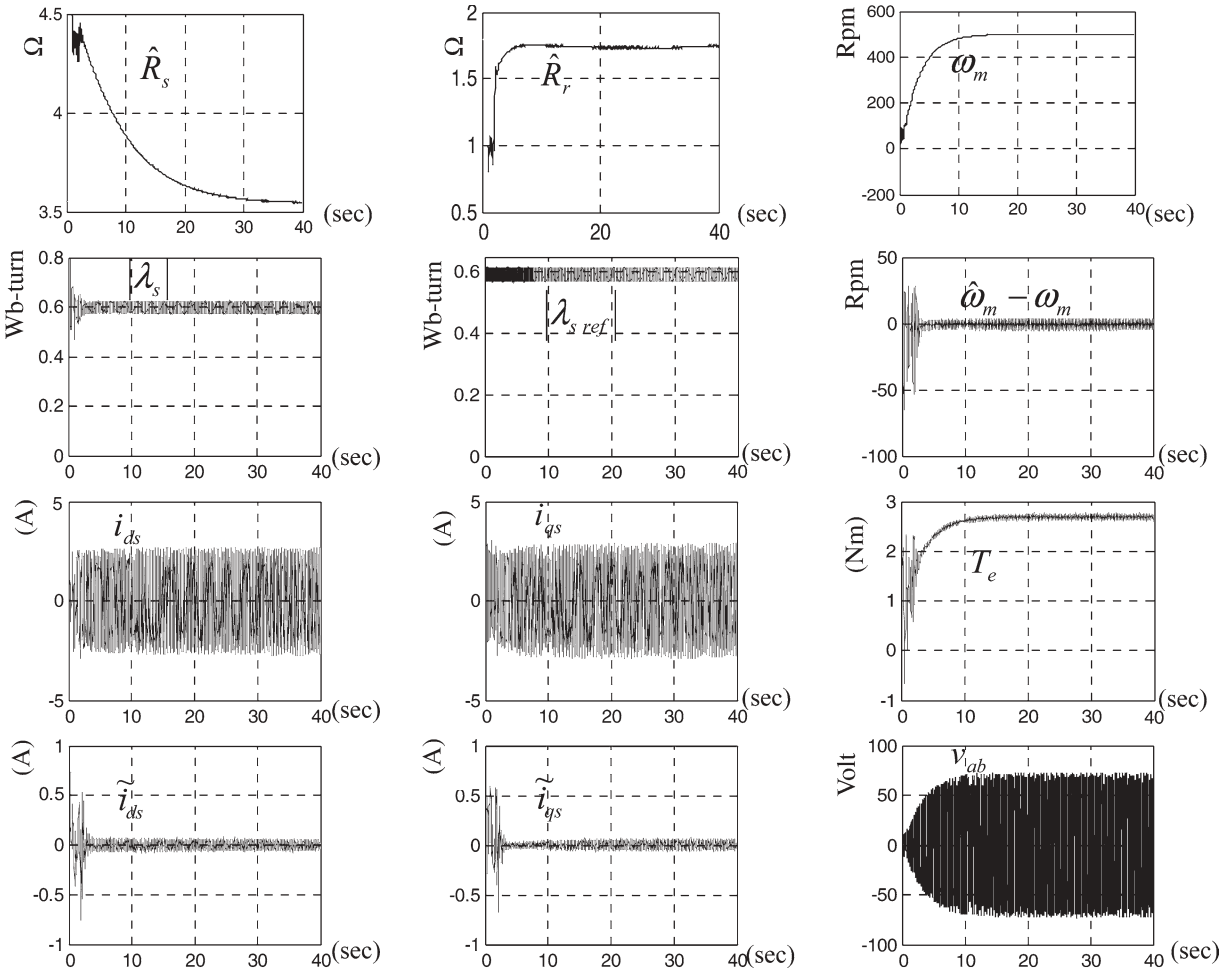

Fig. 6 Simulation results: nonlinear observer behavior in the IM medium speed operating region

$R_s = 1.3 * R_{sn}$ where R_{sn} is the nominal stator resistance. In addition, from Figs. 6 and 7, it is also seen that the estimated stator and rotor resistances respectively converge to their real values.

6 Experimental system and results

6.1 Experimental system setup

For practical evaluation of the actual system performance, a PC-based prototype is built and tested. The experimental setup regarding to overall system block diagram shown in Fig. 8 consists of the following elements: a 2.5 kW squirrel cage induction motor and 2.5 kW DC Generator; Voltage source inverter and its isolation board, 24 bit Digital Input–Output card, 32-channel ADVANECH A/D converter card, FPGA board and a PC-586 computer as a host for commanding signal, estimating parameters, and viewing the waveforms. The 2.5 kW induction motor parameters are reported in Table 1.

The induction motor is supplied by a three-phase 5 kW inverter with a symmetrical two level space vector pulse width modulation (SVPWM) using a Xilinx SPARTANII FPGA with switching frequency of 5 kHZ.

The FPGA board communicates with PC via the digital AXIOM AX5500P I/O board. The use of FPGA system makes it possible to relate parts of the control system using hardware, which unloads the processor from parts of the assigned tasks. FPGA in experimental setup realizes the following functions: pattern generating for control of IGBT switches based on SVM technique, providing a dead time in switching pattern of power switches in a three-phase voltage source inverter, generating sampling pulse of the A/D card, shutting down of inverter in the case of emergency signals and PC hanging condition, control of break IGBT for DC link capacitor protection and data transmission between PC and drive system.

The inverter has been designed specifically for this experiment, using low loss IGBT module SKM40GD124D (with 40 A, 1200 Vratings) and the driving system has been designed using fast and intelligent IGBT drivers, HCPL 316J, which guarantee separation between the inverter and control system. The DC link voltage and stator phase currents and voltages are measured by Hall-type LEM sensors. All measured electrical

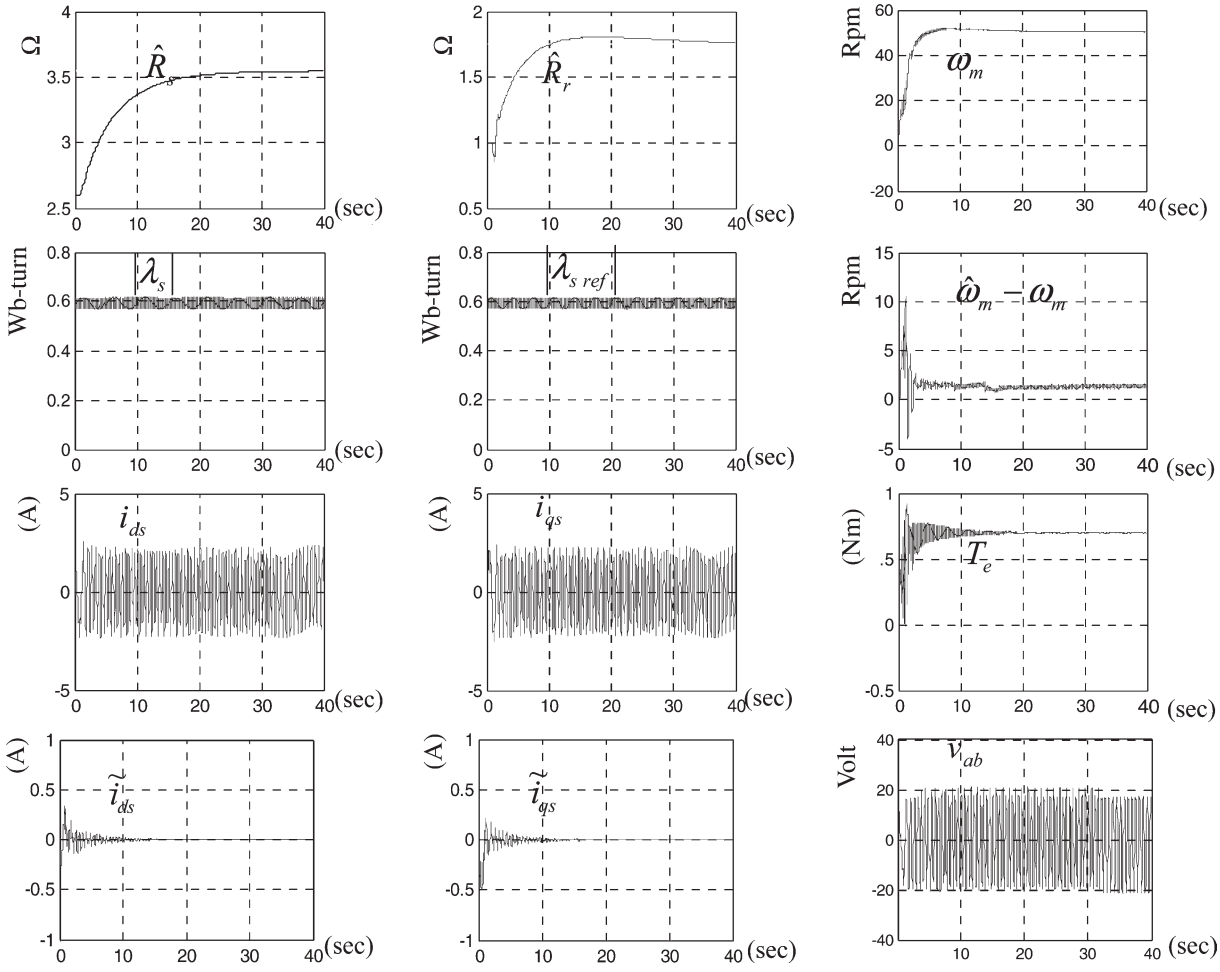

Fig. 7 Simulation results: nonlinear observer behavior in the IM low speed operating region

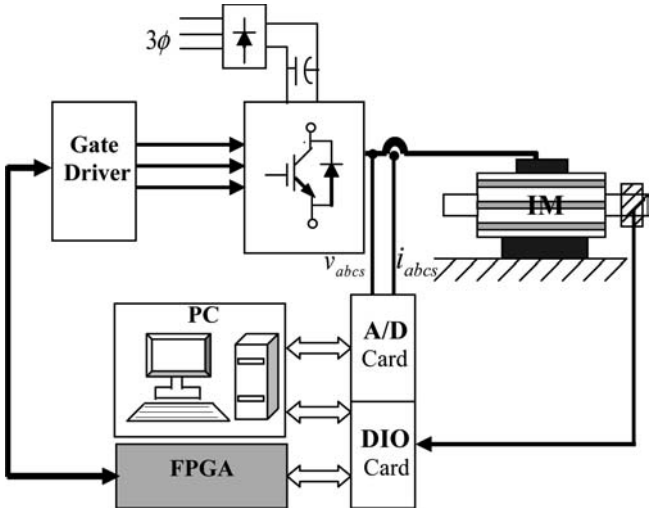

Fig. 8 Experimental setup

signals are filtered by analog second-order low pass filters with cut off frequency of about 2.5 kHz and converted to digital by an 11-bit A/D converter with 10 μs conversion time. The motor speed signal is measured for comparing and monitoring using a AUTONICs incremental encoder with 2000 pulses per round.

6.2 Experimental results

To show the validity and effectiveness of the proposed control approach, the same control objectives as the simulation are adopted. The controller and observer gains are all the same as used in system simulation. The experimental results were obtained respectively for the IM torque, stator flux and speed control as shown in Figs. 9, 10, and 11. A close agreement can be seen between these results and those in Figs. 3, 4, and 5.

Using the proposed adaptive nonlinear observer, the IM speed sensorless performance for 500 rpm and 50 rpm are respectively shown in Figs. 12 and 13. A little disagreement between these results and the corresponding simulation results shown in Figs. 6 and 7 can be explained because of inaccuracies that exist in our data accusation system, inverter power switch dead times, FPGA based SVPWM voltage

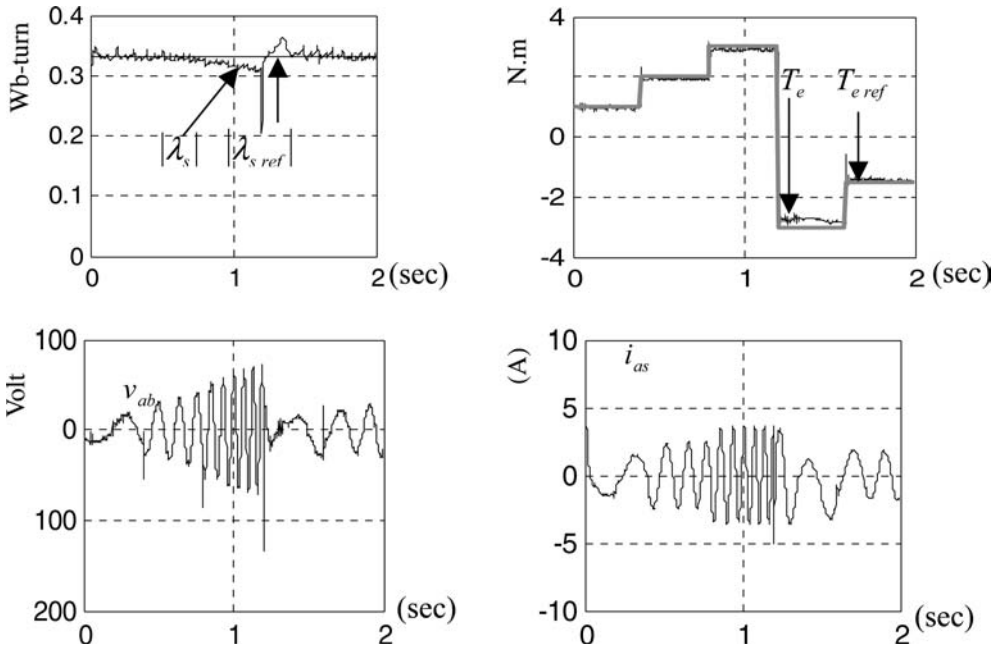

Fig. 9 Experimental results: IM torque control

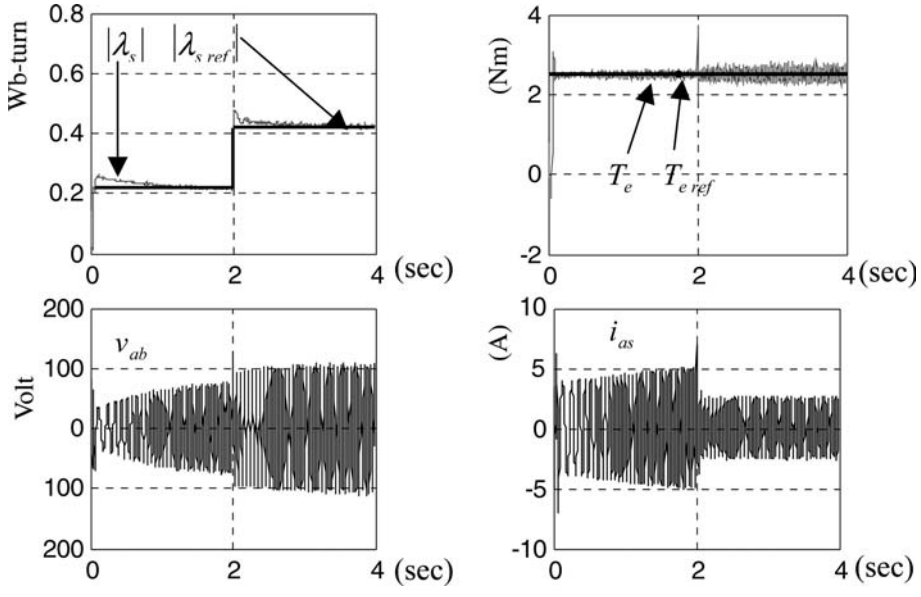

Fig. 10 Experimental results: IM stator flux control

source inverter effects as also because of magnetic saturation and motor iron loss resistance that are not taken into account in our system modeling.

7 Conclusions

A simple DTC-SVM approach has been presented for an adjustable speed sensorless IM drive which is supplied by a two-level SVPWM inverter. According to this control approach, the PWM inverter reference voltage vector is generated by a conventional PI predictor. In addition, the IM torque reference signal is generated by a simple PI speed controller. A novel adaptive nonlinear stator flux observer is developed in order to detect the rotor speed, rotor and stator resistances simultaneously. The stability of this observer is proved by Lyapunov stability theory. The validity of the proposed nonlinear adaptive control method has been shown by simulation and experimental results. A little disagreement seen between these two sets of results can be explained by inaccuracies that exist in the drive system current and voltage acquisition errors, nonlinear characteristics of the SVPWM

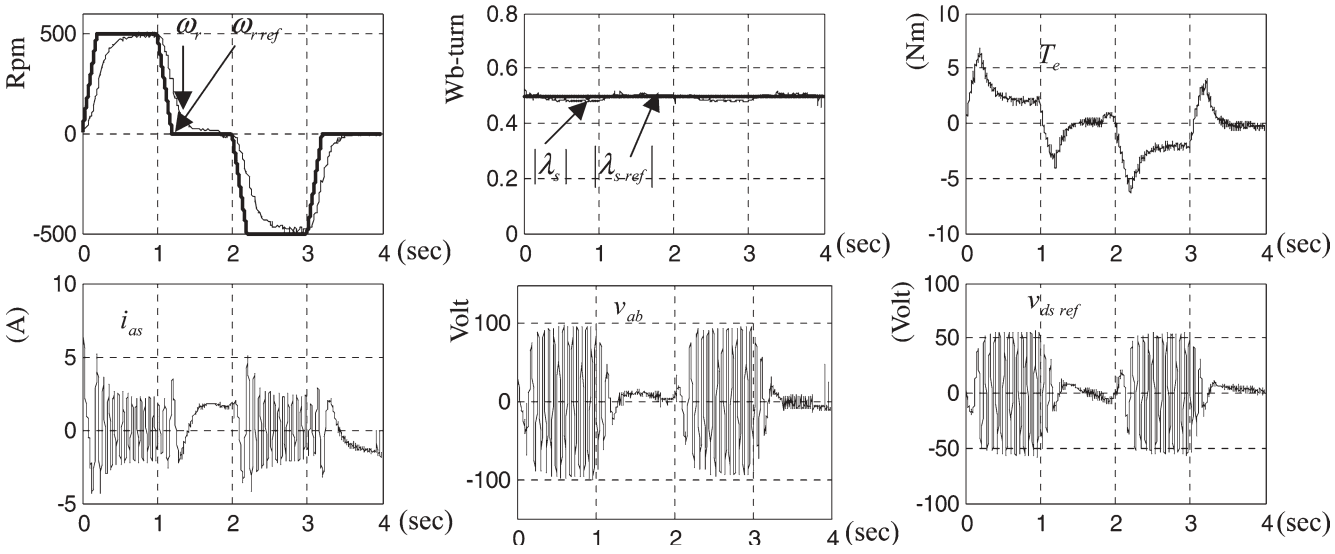

Fig. 11 Experimental results: IM speed control

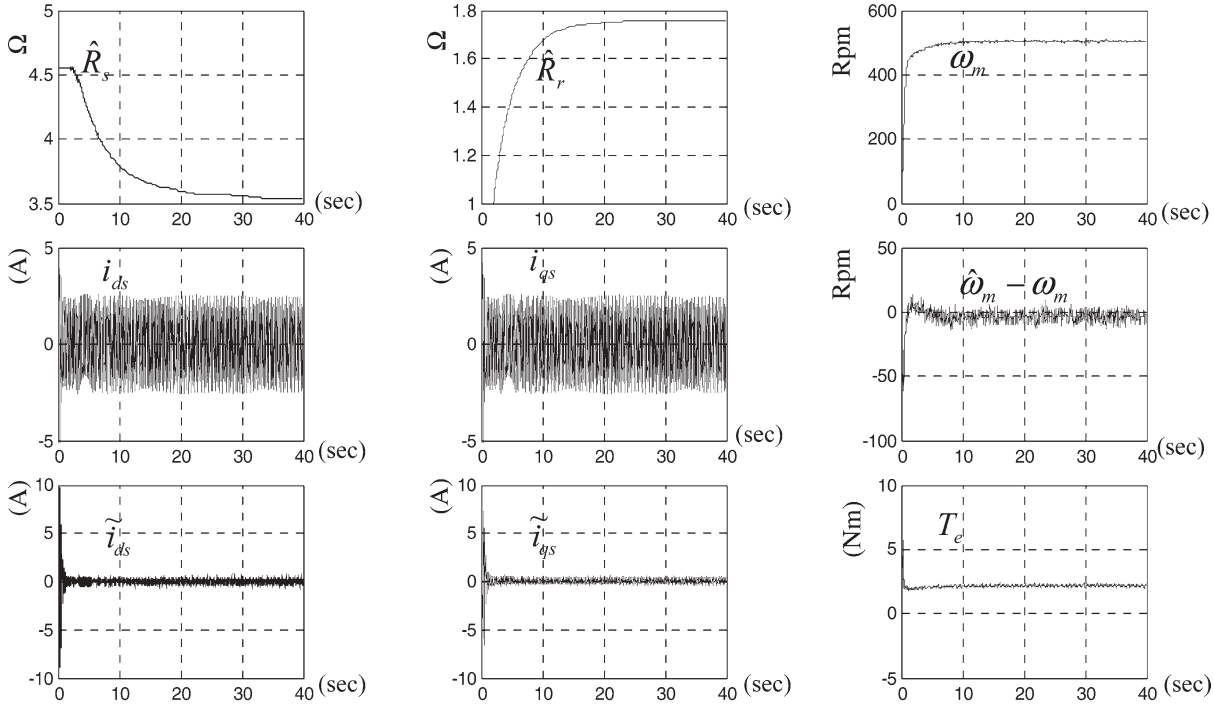

Fig. 12 Experimental results: nonlinear observer behavior in the IM medium speed operating region

inverter, dc offset and drift effects on the stator flux estimation, gain unbalance of the current acquisition channels, residual switching harmonics of the fundamental current signals and finally because of the magnetic saturation and motor iron loss that are not taken in to account in our system modeling.

References

1. Takahashi I, Ohmori Y (1998) High-performance direct torque control of induction motor. IEEE Trans Ind Appl 25(2):257–264
2. Casadei D, Profumo F, Serra G, Tani A (2002) FOC and DTC: two viable schemes for induction motors torque control. IEEE Trans Power Electron 17(5):779–787
3. Noguchi T, Yamamoto M, Kondo S, Takashi I (1997) High frequency switching operation of PWM switching inverter for direct torque control of induction motor. In: Conference record IEEE IAS annual meeting, pp 775–780
4. Lee KB, Song JH, Choy I, Yoo JY (2002) Torque ripple reduction in DTC of induction motor driven by three-phase inverter with low switching frequency. IEEE Trans Power Electron 17(2):255–264
5. Nash NJ (1997) Direct torque control induction motor vector control without an encoder. IEEE Trans Ind Appl 3:333–341

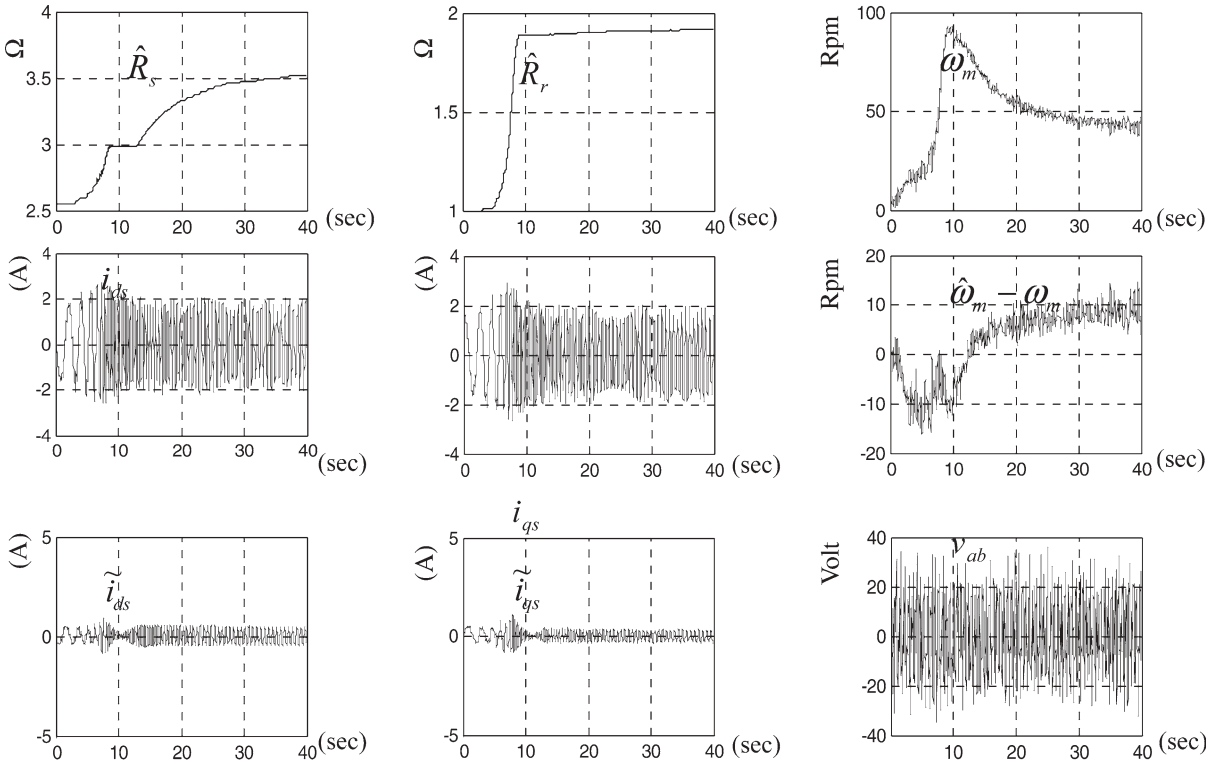

Fig. 13 Experimental results: nonlinear observer behavior in the IM low speed operating region

6. Lascua C, Trzynadlowski AM (2002) Combining the principles of sliding mode, direct torque control and space vector modulation. IAS02 3:2073–2079
7. Lai YS, Chen JH (2001) A new approach to direct torque control of induction motor for constant inverter switching frequency and torque ripple reduction. IEEE Trans Energy Conver 16(3):220–227
8. Swierczyn'ski D, Kazmierkonwski MP (2002) Direct torque control of permanent magnet synchronous motor (PMSM) using space vector modulation (DTC-SVM) simulation and experimental results. IECON02 1:751–755
9. Guidi A, Umida H (1999) A sensorless induction motor drive for low speed applications using a novel stator resistance estimation method. Presented at the IEEE-IAS Annual Meeting, Phoenix, AZ
10. Zhen L, Xu, L (1998) Sensorless Field orientation control of induction machines based on a mutual MRAS scheme. IEEE Trans Ind Electron 45(5):824–831
11. Murai, Gohshi Y, Matsui K, Hosono I (1992) High frequency split zero-vector PWM with harmonic reduction for induction motro drive. IEEE Trans Ind Appl 28(1):105–112
12. Marino R, Tomei P (1995) Nonlinear control design—geometric, adaptive and robust. Prentice-Hall, Englewood Cliffs, NJ, USA
13. Kubota H, Matsuse K (1994) Speed sensorless field-oriented control of induction motor with rotor resistance adaptation. IEEE Trans Ind Appl 30(5):1219–1224
14. Jeon SH, Oh KK, Choi JY (2002) Flux observer with online tuning of stator and rotor resistances for induction motors. IEEE Trans Ind Electron 49(3):653–664